

Impact of Monoatomic Vacancies in 2D Materials on the Performance of Magnetic Tunnel Junction Devices: Insights from Configurations and Interface Interactions

Halimah Harfah,^{1,*} Yusuf Wicaksono,^{2,†} Gagus Ketut Sunnardianto,^{3,4,5} Muhammad Aziz Majidi,⁶ and Koichi Kusakabe⁷

¹*Graduate School of Engineering Science, Osaka University, 1-3 Machikaneyama-Cho, Toyonaka, Osaka 560-0043, Japan*

²*RIKEN Cluster for Pioneering Research (CPR), 2-1 Hirosawa, Wako, Saitama 351-0198, Japan*

³*Research Center for Quantum Physics, National Research and Innovation Agency of Indonesia (BRIN), Tangerang Selatan, Banten, 15314, Indonesia*

⁴*Research Collaboration Center for Quantum Technology 2.0, National Research and Innovation Agency of Indonesia (BRIN), Bandung 40132, Indonesia*

⁵*School of Materials Science and Engineering, Nanyang Technological University, 50 Nanyang Avenue, Singapore 639798, Singapore*

⁶*Department of Physics, Faculty of Mathematics and Natural Sciences, Universitas Indonesia, Kampus UI Depok, Depok 16424, Indonesia.*

⁷*School of Science, Graduate School of Science, University of Hyogo 3-2-1 Kouto, Kamigori-cho, Ako-gun, 678-1297, Hyogo, Japan.*

(Dated: April 4, 2024)

We investigate the impact of monoatomic vacancies in 2D materials on the performance of magnetic tunnel junction (MTJ) devices using first-principles calculations within Density Functional Theory (DFT). Specifically, we analyze the influence on hexagonal boron nitride (hBN) with various layer configurations, uncovering distinct transmission probability patterns. Transmission calculations were conducted using the Landauer-Büttiker formula employing the Non-Equilibrium Green's Function (NEGF) method. In the Ni/hBN(V_B)-hBN/Ni system, a significant reduction in transmission probability was observed compared to non-vacancy configurations. However, when two hBN vacancies were considered, creating the Ni/hBN(V_B)-hBN(V_B)/Ni MTJ system, a new transmission channel mediated by vacancy localized states emerged. The introduction of a monoatomic boron vacancy in the middle hBN layer of the Ni/3hBN/Ni system revealed nuanced effects on the transmission probability, highlighting alterations in the spin minority and majority channels. Additionally, we explore the monoatomic vacancy in the graphene layer in the Ni/hBN-Gr-hBN/Ni MTJ, uncovering a unique transmission channel influenced by the proximity effect. Our findings suggest that the creation of monoatomic vacancies on the insulator barrier of 2D materials induces distinctive characteristics shaped by the interaction between the surface state of the electrode and the localized state of the monoatomic vacancy layer in the MTJ system.

INTRODUCTION

Magnetic tunnel junctions (MTJs) have attracted significant attention in the realm of spintronics, owing to their diverse array of potential applications ranging from logic devices to magnetic sensors [1–6]. A critical factor in optimizing MTJ performance is the tunneling magnetoresistance (TMR) ratio, wherein MgO has emerged as the predominant choice for the tunnel barrier material. For instance, the CoFeB/MgO/CoFeB MTJ configuration has showcased remarkable TMR values, reaching as high as 1100% at 4.2 K [7]. However, the pursuit of downsizing these devices by reducing the barrier thickness has often been impeded by a concomitant decrease in TMR, sometimes plummeting to 55%, primarily attributed to the presence of uncontrollable defects within the MgO tunnel barrier [8, 9].

Conversely, researchers have been actively exploring alternatives to MgO, seeking to replace it with 2D materials as a means of device miniaturization. The potential of 2D materials such as graphene (Gr) or hexagonal boron nitride (hBN) as MTJ spin valves has been thor-

oughly investigated [10–17]. One such approach involves employing a monolayer or a few layers of hBN as the tunnel barrier, sandwiched between ferromagnetic electrodes to form MTJ structures [18–28]. In the Ni/monolayer hBN/Ni MTJ system, the interaction between Ni and N atoms at the interface can lead to pd -hybridization, allowing electrons at the Fermi energy to easily pass through the monolayer hBN as a tunnel barrier [13]. This electron transmission is primarily due to propagating-wave electrons. In contrast, when multilayer hBN serves as the tunnel barrier, the transmission of electrons through the hBN insulator barrier is facilitated by the Ni d_{z^2} -orbital surface state and the proximity effect induced on the hBN layer [14]. This finding emphasizes the pivotal role played by the proximity effect within 2D materials in modulating electron tunneling capacity. Interestingly, unlike conventional thin-film materials such as MgO, modified 2D materials, engineered through the introduction of monoatomic vacancies, exhibit a spectrum of unique physical and chemical properties [29–32]. These distinct characteristics may mediate novel transmission phenomena not observed in MgO-based MTJs.

In the field of spintronics, investigating the impact of monoatomic vacancies in two-dimensional (2D) materials on the performance of MTJ devices is of critical importance [33–36]. To understand how single-atom defects (monoatomic vacancies) in two-dimensional (2D) materials affect the transmission properties of MTJs, we use a theoretical framework based on Density Functional Theory (DFT). This allows us to explore the complex relationship between the electronic properties and device performance. We examine the transmission properties using the Landauer-Büttiker formula. The Non-Equilibrium Green's Function (NEGF) method is then employed to gain insights into the transport properties of the systems. We focused on hexagonal boron nitride (hBN), a well-known insulator, and explored how different layer arrangements within the MTJ device affect its performance. By controlling monoatomic vacancies and altering the layer structures, we observed significant changes in the transmission probability, especially in the spin-dependent channels. Furthermore, we incorporated graphene layers within the MTJ design and investigated how monoatomic vacancies impact the transmission properties in these hybrid systems. This study deepens our understanding of the fundamental mechanisms governing electron transport in MTJ devices and provides practical guidance for designing and optimizing future spintronic devices. By investigating the impact of monoatomic vacancies in 2D materials on device performance, we aim to advance spintronics towards devices with enhanced functionality and efficiency.

COMPUTATIONAL METHOD

In this work, we used a 3×3 supercell to model the MTJ systems. To introduce defects, a monoatomic boron vacancy (V_B) was deliberately created within the hBN layer, as depicted in Figure 1(a). Additionally, a monoatomic vacancy was introduced into the graphene layer, as illustrated in Figure 1(b). We explored various stacking configurations of hBN(V_B) layers, including hBN(V_B)/hBN, hBN(V_B)/hBN(V_B), and hBN/hBN(V_B)/hBN, as shown in Figures 1(c), (d), and (e), respectively. Furthermore, we investigated the hBN/Gr/hBN stacking with different vacancy configurations, where the vacancy was positioned on the graphene layer, as depicted in Figure 1(f). The study primarily focused on evaluating the significance of localized states in spin-dependent electron tunneling between two ferromagnetic electrodes, with nickel chosen as the electrode material. Given that the anti-parallel configuration (APC) is known to exhibit low transmission probability due to the spin-blocking effect, our analysis primarily focused on the parallel configuration (PC) state of the MTJ, where the magnetic moments of the upper and lower Ni electrodes were oriented parallelly upward.

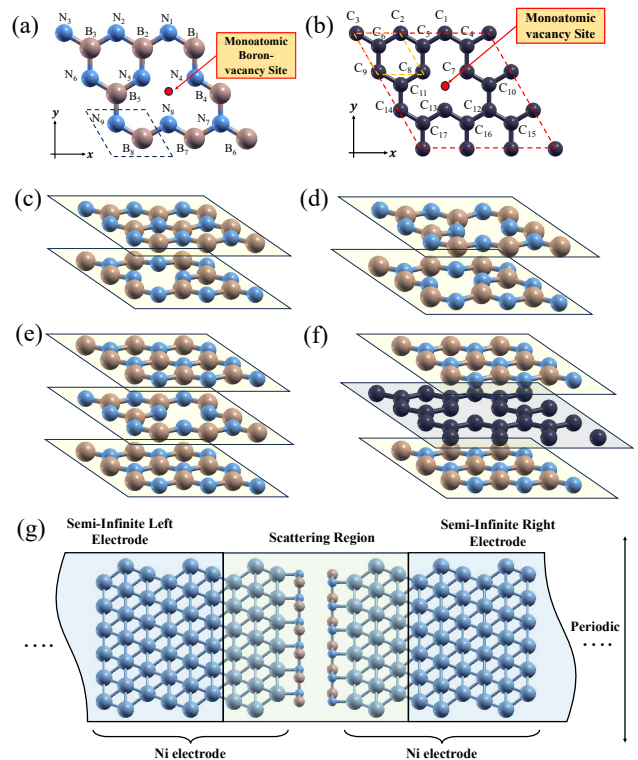


FIG. 1. A 3×3 unit cell of (a) hBN with a monoatomic boron vacancy (V_B), (b) graphene (Gr) with a vacancy, (c) hBN(V_B)/hBN, (d) hBN(V_B)/hBN(V_B), (e) hBN/hBN(V_B)/hBN, and (f) hBN/Gr(V)/hBN used in the calculations. Blue, black, and pink color balls represent N, C, B atoms, respectively. (g) The setup to calculate the tunneling transmission probability of the aforementioned tunnel barrier where Ni is used as electrodes. The scattering region comprises a three-layer Ni/tunnel barrier/three-layer Ni, and the left and right electrodes comprise six Ni layers. Visualization was performed using XCrySDen [37]

The SIESTA package [38, 39] was utilized for various calculations, encompassing structural equilibrium determination, assessment of magnetic properties, mapping of spin-charge density, and determination of the local density of states (LDOS) utilizing spin-polarized DFT. Electron-ion interaction within the generalized gradient approximation (GGA) was modeled using the Troullier–Martins [40] pseudopotential and the Perdew–Burke–Ernzerhof functional, specifically the PBEsol functional [41]. A basis set incorporating double-zeta and polarization was employed [42–44]. The atomic positions were relaxed with a force tolerance of 0.01 eV/Å, and a Monkhorst–Pack k-mesh of $36 \times 36 \times 1$ was utilized for calculations, with a mesh cutoff of 500 Ry. Additionally, van der Waals interactions between hBN and graphene were accounted for by integrating a Grimme-type dispersion potential [45].

The tunneling transmission probability was computed using the Landauer-Büttiker formalism within the NEGF

method. The setup for calculating the transmission probability is depicted in Figure 1(g). The spin-dependent current was determined utilizing the Landauer-Büttiker equation:

$$I^{\uparrow(\downarrow)} = \frac{e}{h} \int_{-\infty}^{\infty} T^{\uparrow(\downarrow)}(E) [f_L(E, \mu) - f_R(E, \mu)] dE, \quad (1)$$

where $f_L(E, \mu)$ ($f_R(E, \mu)$) represents the right (left) moving electrons injected from the left (right) electrode, and μ_L (μ_R) denotes the chemical potentials of the left (right) electrodes, both assumed to be at the Fermi level (E_F) due to the zero bias voltage. The transmission probability, T , as a function of energy, E , is described by the Green's function:

$$T^{\uparrow(\downarrow)}(E) = \text{Tr} \left\{ \left[\Gamma_L G^R \Gamma_R G^A \right] \right\}, \quad (2)$$

where Γ_L (Γ_R) represents the coupling matrix of the left (right) electrode, and G^R (G^A) denotes the retarded (advanced) Green's function of the central region.

RESULTS AND DISCUSSION

Influence of Monoatomic Boron Vacancy in One or Two hBN in Ni/2hBN/Ni MTJ

To examine the impact of a monoatomic boron vacancy in hBN on the functionality of an MTJ device, we investigated two potential configurations: Ni/hBN(V_B)-hBN/Ni and Ni/hBN(V_B)-hBN(V_B)/Ni MTJ systems. The presence of a monoatomic boron vacancy induces magnetization in the hBN layer. This phenomenon is attributed to the unpaired electron of the nitrogen atoms

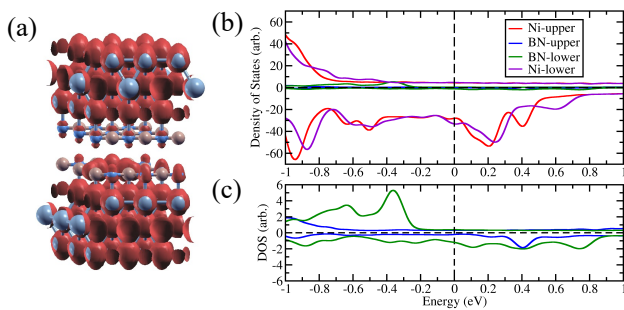


FIG. 2. (a) The 3×3 Ni/hBN/hBN(V_B)/Ni SCDM (red color represents spin-up electron density). Visualization was performed using XCrySDen [37]. (b) LDOS for Ni-upper, hBN-upper, hBN-lower (hBN with V_B), and Ni-lower layers in PC configuration. The positive (negative) value of DOS represents the spin majority (minority) channel. (c) A zoom on the lower energy of LDOS in (b).

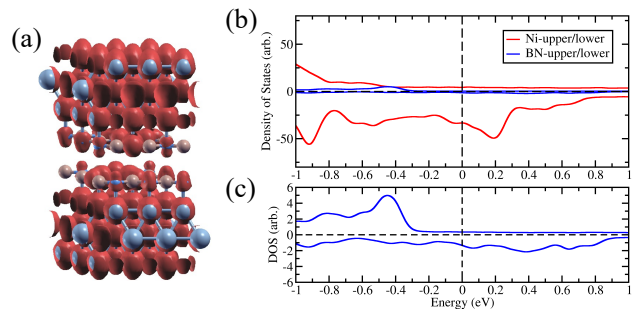


FIG. 3. (a) The 3×3 Ni/hBN(V_B)/hBN(V_B)/Ni SCDM (red color represents spin-up electron density). Visualization was performed using XCrySDen [37]. (b) LDOS for Ni-upper/lower and hBN-upper/lower (which both have V_B) in the PC configuration. The positive (negative) value of DOS represents the spin majority (minority) channel. (c) A zoom on the lower energy of LDOS in (b).

at the vacancy site, which fails to form a σ -bond with the boron atom. We observe vacancy-induced magnetization in both Ni/hBN(V_B)-hBN/Ni and Ni/hBN(V_B)-hBN(V_B)/Ni MTJs, as depicted in Figures 2(a) and 3(a), respectively, through spin charge density mapping (SCDM). Notably, the SCDM reveals dominant spin-up electron density in the localized state near V_B , aligned parallel to the spin-up magnetization direction of the Ni slabs. This alignment signifies a strong ferromagnetic coupling between the magnetic moment at the vacancy and the Ni slabs. Furthermore, a short-range magnetic interaction between the localized state and neighboring nitrogen atoms is evident from the damping of spin-up electron density amplitude. This damping occurs in regions where spin-up electron density concentrates near the vacancy but decreases for nitrogen atoms farther away. The emergence of vacancy-induced magnetization in hBN(V_B) is expected to alter its electronic structure and the propagation of Ni dz^2 -orbital surface state through the insulator barrier of two hBN layers.

Initially, we examined the influence of V_B on the electronic structure of the MTJ system using Ni/hBN(V_B)-hBN/Ni. This configuration allowed for a direct comparison between pristine hBN, hybridized with the upper Ni slab, and hBN(V_B), hybridized with the lower Ni slab. Figure 2(b) displays the local density of states (LDOS) of the upper and lower Ni slabs, pristine upper hBN, and lower hBN with V_B in the PC configuration. A notable difference in LDOS between the upper and lower Ni slabs is observed, stemming from the modification of pd -hybridization at the interface of hBN(V_B)/Ni. This modification is evidenced by the DOS peak at $E - E_F = 0.4$ eV in the spin minority channel, corresponding to hybridization at the Ni/hBN interface between the Ni dz^2 orbital and the nitrogen p_z orbital. This peak also appears in the spin majority channel at approximately $E - E_F = -1.0$ eV, consis-

tent with previous findings[14]. However, in the lower Ni slab, hybridized with hBN(V_B), the DOS peak in the spin minority channel at $E - E_F = 0.4$ eV is reduced due to the electron localization at the vacancy site. A similar reduction is observed in the spin majority channel around $E - E_F = -1.0$ eV. The disparity is more pronounced between the upper and lower hBN layers, as shown in Figure 2(c). In the upper hBN, a nearly insulating gap dominates the DOS, with a peak only appearing at $E - E_F = 0.4$ eV for the spin minority channel and around $E - E_F = -1.0$ eV for the spin majority channel, arising from pd -hybridization. Conversely, the lower hBN containing V_B exhibits a DOS peak in the same energy range as the upper hBN, along with additional states. In the spin majority channel, a higher DOS peak is observed from $E - E_F = -0.9$ to -0.2 eV, with the highest and second-highest DOS at $E - E_F = -0.38$ and -0.65 eV, respectively. Meanwhile, in the spin minority channel, a broad range of new states emerges from $E - E_F = -1.0$ to 1.0 eV. The higher occupancy of states in the spin majority channel compared to the minority channel corresponds to the spin-up magnetization of hBN(V_B) due to the vacancy.

The modification of the LDOS in the lower Ni and hBN layers directly affects the probability of electron transmission. As previously mentioned, in a two-layer hBN MTJ system, electron transmission primarily occurs through the Ni surface state. Figure 4 illustrates a prominent transmission peak at $E - E_F = 0.38$ eV (-0.98 eV) for spin-down (spin-up) electrons, consistent with previous findings. This high transmission is attributed to electron transmission through the Ni d_{z^2} orbital surface state. However, in the Ni/hBN/hBN(V_B)/Ni MTJ structure, the decreased Ni d_{z^2} orbital DOS leads to a significant reduction in electron transmission for both spin-up and spin-down electrons. Conversely, in the Ni/hBN(V_B)-hBN(V_B)/Ni MTJ, identical LDOS in both the upper and lower Ni and hBN layers, as shown in Figure 3(b) and (c), similarly reduces electron transmission probability for spin-down (spin-up) electrons at $E - E_F = 0.38$ eV (-0.98 eV) while creating a new transmission channel for spin-down (spin-up) electrons from $E - E_F = 0.5$ eV (-0.85 eV) to 0.8 eV (-0.4 eV). This suggests that the newly created states in hBN(V_B) mediate electron transmission not only for the Ni d_{z^2} orbital surface state but also for another orbital surface state.

We note that the Ni/hBN(V_B)-hBN(V_B)/Ni MTJ introduces a new transmission channel when the hBN(V_B) layers are in close proximity. However, as the separation between hBN(V_B) layers increases, the intensity of the transmission channel decreases and eventually disappears, resembling the transmission observed in Ni/hBN(V_B)-hBN/Ni.

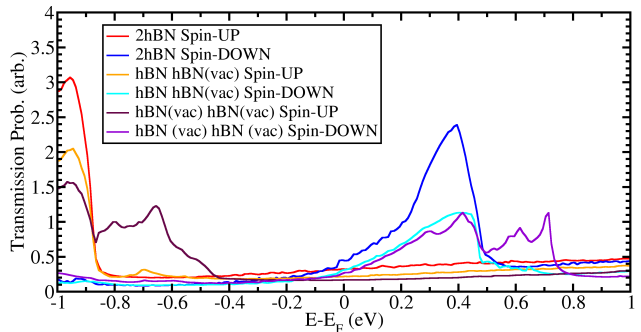


FIG. 4. Comparison of transmission probability for Ni/2hBN/Ni, Ni/hBN(V_B)/hBN/Ni, and Ni/hBN(V_B)/hBN(V_B)/Ni MTJs.

Interaction Between Ni's Surface State at Interface with Localized State of 2D Materials Vacancy

In the preceding section, we examined the influence of V_B on the electronic structure of both the hBN and Ni layers at the Ni/hBN interface. Here, we delve into the interaction between the surface state of Ni at the interface, which remains unaltered, and the isolated localized state of the middle hBN layer in the Ni/hBN/hBN(V_B)/hBN/Ni MTJ.

Figure 5(a) illustrates the spin charge density mapping (SCDM) of the Ni/hBN/hBN(V_B)/hBN/Ni MTJ, indicating that the hBN(V_B) in the middle possesses an induced magnetic moment. A strong magnetic moment is observed at the vacancy site, aligned parallel to the Ni slab, suggesting magnetic interaction between the hBN(V_B) and Ni slab despite lacking a direct interface. The local density of states (LDOS) of the Ni slab, hBN at the interface, and hBN(V_B) is depicted in Figures 5(b) and (c). The LDOS analysis reveals that the hBN(V_B) in the middle does not alter the DOS of the Ni layer at the interface or the hBN at the interface. However, the DOS of the hBN(V_B) exhibits spin polarization, evident from the Stoner gap. The newly created state from the vacancy shows some overlap with the surface state of the Ni d_{z^2} orbital at $E - E_F = 0.42$ eV (-0.9 eV) for the spin minority (majority) channel.

The transmission probability of the Ni/hBN/hBN(V_B)/hBN/Ni MTJ is displayed in Figure 7(a). No new transmission channel is observed. Instead, an increment (reduction) in the transmission probability is noted for the spin majority (minority) channel at $E - E_F = -0.9$ eV (0.42 eV) compared to the Ni/3hBN/Ni MTJ. This indicates that the Ni d_{z^2} orbital solely affects the occupied state of the localized state. The reduction in transmission probability in the spin minority channel, due to the Ni d_{z^2} orbital surface state, does not interact with the proximity effect, which exhibits spin-up electron localization. Conversely, the

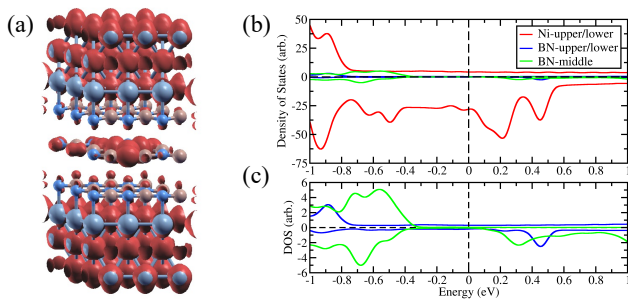


FIG. 5. (a) The 3×3 Ni/hBN/hBN(V_B)/hBN/Ni SCDM (red color represents spin-up electron density). Visualization was performed using XCrySDen [37]. (b) Local density of states (LDOS) for Ni-upper/lower and hBN-upper/lower (hBN without V_B), and hBN-middle (hBN with V_B) in PC configuration. The positive (negative) value of DOS represents spin majority (minority) channel. (c) The zoom on lower energy of LDOS in (b).

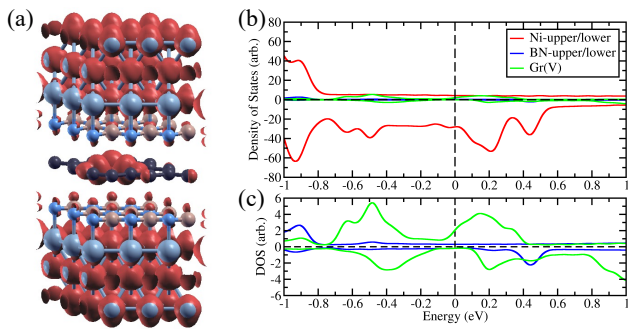


FIG. 6. (a) The 3×3 Ni/hBN/Gr(V)/hBN/Ni SCDM (red color represents spin-up electron density). Visualization was performed using XCrySDen [37]. (b) LDOS for Ni-upper/lower, hBN-upper/lower, and Gr(V) in PC configuration. The positive (negative) value of DOS represents spin majority (minority) channel. (c) The zoom on lower energy of LDOS in (b).

spin majority channel of the Ni dz^2 orbital surface state propagates through the localized state, resulting in an increment in the transmission probability of spin-up electrons.

In a complementary investigation, we introduced a monoatomic vacancy in the graphene layer to create the Ni/hBN/Gr(V)/hBN/Ni MTJ. Similar to the hBN(V_B) in Ni/hBN/hBN(V_B)/hBN/Ni MTJ, the graphene with a vacancy exhibits an induced magnetic moment and ferromagnetic interaction with the Ni slab, as shown in Figure 6(a). Furthermore, the vacancy in graphene does not modify the DOS of the Ni layer at the interface or the hBN layer at the interface, as depicted in Figures 6(b) and (d). Interestingly, a decrease in spin-down electron transmission at higher energy, akin to the Ni/hBN/hBN(V_B)/hBN/Ni MTJ system, is observed. In the Ni/hBN/Gr(V)/hBN/Ni MTJ, the vacancy in

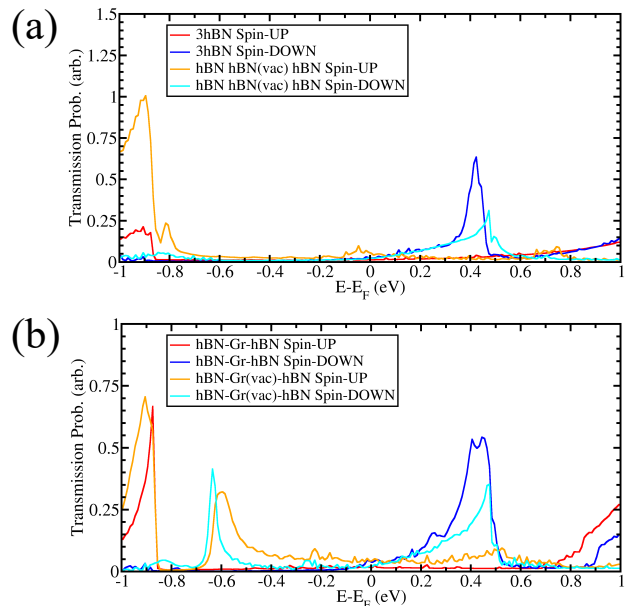


FIG. 7. Transmission probability comparison between (a) Ni/3hBN/Ni and Ni/hBN/hBN(V_B)/hBN/Ni MTJs, and between (b) Ni/hBN/Gr/hBN/Ni and Ni/hBN/Gr(V)/hBN/Ni MTJs.

graphene creates a new transmission channel for both spin-up and spin-down electrons within the same energy range, around $E - E_F = -0.6$ eV, as shown in Figure 7(b). This unique transmission channel originates from the proximity effect, which interacts with the localized state as well as the π -orbital of the graphene layer. However, this interaction occurs at the occupied state, implying that the surface state not only propagates through Gr(V) mediated by the localized state but can also be redistributed within the graphene layer through graphene's π -orbital. We anticipate the tunneling magnetoresistance (TMR) ratio at $E - E_F = -0.6$ eV to exceed 1200%, as found in Ni/hBN/Gr/hBN/Ni.

CONCLUSION

In this study, we investigated the impact of a monoatomic vacancy in 2D materials on the performance of an MTJ device. Initially, we explored bilayer hexagonal boron nitride (hBN) configurations, considering Ni/hBN(V_B)-hBN/Ni and Ni/hBN(V_B)-hBN(V_B)/Ni MTJ systems. The transmission probability was notably reduced in the Ni/hBN(V_B)-hBN/Ni configuration compared to the pristine bilayer hBN system. Conversely, in the Ni/hBN(V_B)-hBN(V_B)/Ni configuration, an additional peak in the transmission probability emerged, indicating a new transmission channel facilitated by the localized state of hBN(V_B)-hBN(V_B).

Subsequently, we introduced a monoatomic boron va-

cancy in the middle hBN layer of the Ni/3hBN/Ni system, creating a Ni/hBN-hBN(V_B)-hBN/Ni MTJ. The presence of the localized state in the middle hBN layer led to a reduction (enhancement) in the transmission probability peak for the spin minority (majority) channel at higher (lower) energy, attributed to the stoner gap created in the middle hBN layer. Consequently, the transmission probability for the spin-majority channel was augmented.

Finally, we investigated the monoatomic vacancy in the graphene layer of the Ni/hBN-Gr-hBN/Ni MTJ. The presence of the graphene vacancy induced a new transmission channel for both the spin-majority and minority channels within the same energy range. This unique transmission channel originated from the proximity effect interacting with the localized state of the graphene layer.

The introduction of a monoatomic vacancy on the insulator barrier of 2D materials in the MTJ system results in unique characteristics determined by the interaction between the surface state of the electrode and the localized state of the monoatomic vacancy layer. This interaction offers promising avenues for tailoring the properties and performance of spintronic devices based on MTJs.

CONFLICTS OF INTEREST

“There are no conflicts to declare”.

ACKNOWLEDGEMENTS

Calculations were performed at the Kyushu University computer center. H.H. gratefully acknowledges the fellowship support from the JSPS. This study was partly supported by the Japan Society for the Promotion of Science (JSPS) KAKENHI (Grant Nos. JP19H00862 and JP16H00914 in the Science of Atomic Layers, 21J22520 in the Grant-in-Aid for Young Scientists, and JP18K03456).

* Corresponding author: harfah.h@opt.mp.es.osaka-u.ac.jp; These authors contributed equally to this work

† These authors contributed equally to this work

- [1] C. Chappert, A. Fert, and F. N. Van Dau, The emergence of spin electronics in data storage, *Nature Materials* **6**, 813 EP (2007).
- [2] H. Dery, P. Dalal, L. Cywiński, and L. J. Sham, Spin-based logic in semiconductors for reconfigurable large-scale circuits, *Nature* **447**, 573 EP (2007).
- [3] J.-G. J. Zhu and C. Park, Magnetic tunnel junctions, *Materials Today* **9**, 36 (2006).
- [4] J. R. Childress and R. E. Fontana, Magnetic recording read head sensor technology, *Spintronics*, *Comptes Rendus Physique* **6**, 997 (2005).
- [5] E. Chen, D. Apalkov, Z. Diao, A. Driskill-Smith, D. Druist, D. Lottis, V. Nikitin, X. Tang, S. Watts, S. Wang, S. A. Wolf, A. W. Ghosh, J. W. Lu, S. J. Poon, M. Stan, W. H. Butler, S. Gupta, C. K. A. Mewes, T. Mewes, and P. B. Visscher, Advances and future prospects of spin-transfer torque random access memory, *IEEE Transactions on Magnetics*, *IEEE Transactions on Magnetics* **46**, 1873 (2010).
- [6] M. Iqbal, N. Qureshi, and G. Khan, *Recent Advancements in 2D-Materials Interface Based Magnetic Junctions for Spintronics*, Vol. 457 (Elsevier, 2018).
- [7] S. Ikeda, K. Miura, H. Yamamoto, K. Mizunuma, H. D. Gan, M. Endo, S. Kanai, J. Hayakawa, F. Matsukura, and H. Ohno, A perpendicular-anisotropy cobe-mgo magnetic tunnel junction, *Nature Materials* **9**, 721 (2010).
- [8] J. C. Leutenantsmeyer, M. Walter, V. Zbarsky, M. Münzenberg, R. R. Gareev, K. Rott, A. Thomas, G. Reiss, P. Peretzki, H. Schuhmann, M. Seibt, M. Czerner, and C. Heiliger, Parameter space for thermal spin-transfer torque, *Spin* **03**, 1350002 (2013).
- [9] W. X. Wang, Y. Yang, H. Naganuma, Y. Ando, R. C. Yu, and X. F. Han, The perpendicular anisotropy of Co40Fe40B20 sandwiched between Ta and MgO layers and its application in CoFeB/MgO/CoFeB tunnel junction, *Applied Physics Letters* **99**, 012502 (2011), https://pubs.aip.org/aip/apl/article-pdf/doi/10.1063/1.3605564/14453243/012502_1_online.pdf.
- [10] Y. Wicaksono, S. Teranishi, K. Nishiguchi, and K. Kusakabe, Tunable induced magnetic moment and in-plane conductance of graphene in ni/graphene/ni nano-spin-valve-like structure: a first principles study, *Carbon* **143**, 828 (2019).
- [11] Y. Wicaksono, H. Harfah, G. K. Sunnardianto, M. A. Majidi, and K. Kusakabe, Colossal in-plane magnetoresistance ratio of graphene sandwiched with ni nanostructures, *RSC Advances* **12**, 13985 (2022).
- [12] Y. Wicaksono, H. Harfah, G. K. Sunnardianto, M. A. Majidi, and K. Kusakabe, Spin-topological electronic valve in ni/hbn-graphene-hbn/ni magnetic junction, *Magnetochemistry* **9**, 113 (2023).
- [13] H. Harfah, Y. Wicaksono, M. A. Majidi, and K. Kusakabe, Spin-current control by induced electric polarization reversal in ni/hbn/ni: A cross-correlation material, *ACS Applied Electronic Materials*, *ACS Applied Electronic Materials* **2**, 1689 (2020).
- [14] H. Harfah, Y. Wicaksono, G. K. Sunnardianto, M. A. Majidi, and K. Kusakabe, High magnetoresistance of a hexagonal boron nitride-graphene heterostructure-based mtj through excited-electron transmission, *Nanoscale Advances* **4**, 117 (2022).
- [15] H. Yu, Z. Shao, Y. Tao, X. Jiang, Y. Dong, J. Zhang, Y. Liu, X. Yang, and D. Chen, Tunable tunneling magnetoresistance in in-plane double barrier magnetic tunnel junctions based on b vacancy h-nb nanoribbons, *Physical Chemistry Chemical Physics* **24**, 3451 (2022).
- [16] A. M. Ukpong, Axial field induced spin response in fe/hbn-based tunnel junctions, *Phys. Rev. B* **100**, 035424 (2019).
- [17] H. Harfah, Y. Wicaksono, G. K. Sunnardianto, M. A. Majidi, and K. Kusakabe, Ultra-thin van der waals magnetic tunnel junction based on monoatomic boron vacancy of hexagonal boron nitride, *Physical Chemistry Chemical Physics* **26**, 9733 (2024).

- [18] M. Piquemal-Banci, R. Galceran, M.-B. Martin, F. Godel, A. Anane, F. Petroff, B. Dlubak, and P. Seneor, 2d-MTJs: introducing 2d materials in magnetic tunnel junctions, *Journal of Physics D: Applied Physics* **50**, 203002 (2017).
- [19] T. M. G. Mohiuddin, E. Hill, D. Elias, A. Zhukov, K. Novoselov, and A. Geim, Graphene in multilayered csp spin valves, *IEEE Transactions on Magnetics* **44**, 2624 (2008).
- [20] P. U. Asshoff, J. L. Sambricio, A. P. Rooney, S. Slizovskiy, A. Mishchenko, A. M. Rakowski, E. W. Hill, A. K. Geim, S. J. Haigh, V. I. Fal'ko, I. J. Vera-Marun, and I. V. Grigorieva, Magnetoresistance of vertical co-graphene-nife junctions controlled by charge transfer and proximity-induced spin splitting in graphene, *2D Materials* **4**, 031004 (2017).
- [21] M. Z. Iqbal, M. W. Iqbal, X. Jin, C. Hwang, and J. Eom, Interlayer dependent polarity of magnetoresistance in graphene spin valves, *J. Mater. Chem. C* **3**, 298 (2015).
- [22] M. Z. Iqbal, M. W. Iqbal, J. H. Lee, Y. S. Kim, S.-H. Chun, and J. Eom, Spin valve effect of nife/graphene/nife junctions, *Nano Research* **6**, 373 (2013).
- [23] J.-J. Chen, J. Meng, Y.-B. Zhou, H.-C. Wu, Y.-Q. Bie, Z.-M. Liao, and D.-P. Yu, Layer-by-layer assembly of vertically conducting graphene devices, *Nature Communications* **4**, 1921 (2013), article.
- [24] F. Li, T. Li, and X. Guo, Vertical graphene spin valves based on $\text{La}_2/3\text{Sr}_1/3\text{MnO}_3$ electrodes, *ACS Applied Materials & Interfaces* **6**, 1187 (2014).
- [25] W. Li, L. Xue, H. D. Abruña, and D. C. Ralph, Magnetic tunnel junctions with single-layer-graphene tunnel barriers, *Phys. Rev. B* **89**, 184418 (2014).
- [26] S. Mandal and S. K. Saha, Ni/graphene/ni nanostructures for spintronic applications, *Nanoscale* **4**, 986 (2012).
- [27] M.-B. Martin, B. Dlubak, R. S. Weatherup, M. Piquemal-Banci, H. Yang, R. Blume, R. Schloegl, S. Collin, F. Petroff, S. Hofmann, J. Robertson, A. Anane, A. Fert, and P. Seneor, Protecting nickel with graphene spin-filtering membranes: A single layer is enough, *Applied Physics Letters* **107**, 012408 (2015), <https://doi.org/10.1063/1.4923401>.
- [28] S. Entani, T. Seki, Y. Sakuraba, T. Yamamoto, S. Takahashi, H. Naramoto, K. Takanashi, and S. Sakai, Magnetoresistance effect in $\text{Fe}_2\text{O}_{\text{Ni}_8}\text{O}/\text{graphene}/\text{Fe}_2\text{O}_{\text{Ni}_8}\text{O}$ vertical spin valves, *Applied Physics Letters*, *Applied Physics Letters* **109**, 082406 (2016).
- [29] T. T. Tran, C. Elbadawi, D. Totonjian, C. Lobo, G. Grosso, H. Moon, D. Englund, M. J. Ford, I. Aharonovich, and M. Toth, Robust multicolor single photon emission from point defects in hexagonal boron nitride, *ACS Nano* **10**, 7331 (2016).
- [30] W. Liu, Z. Li, Y. Yang, S. Yu, Y. Meng, Z. Wang, Z. Li, N. Guo, F. Yan, Q. Li, J. Wang, J. Xu, Y. Wang, J. Tang, C. Li, and G. Guo, Temperature-dependent energy-level shifts of spin defects in hexagonal boron nitride, *ACS Photonics* **8**, 1889 (2021).
- [31] V. Ivády, G. Barcza, G. Thiering, S. Li, H. Hamdi, J.-P. Chou, Ö. Legeza, and A. Gali, Ab initio theory of the negatively charged boron vacancy qubit in hexagonal boron nitride, *npj Computational Materials* **6**, 41 (2020).
- [32] Z. Mu, H. Cai, D. Chen, J. Kenny, Z. Jiang, S. Ru, X. Lyu, T. S. Koh, X. Liu, I. Aharonovich, and W. Gao, Excited-state optically detected magnetic resonance of spin defects in hexagonal boron nitride, *Phys. Rev. Lett.* **128**, 216402 (2022).
- [33] P. U. Asshoff, J. L. Sambricio, S. Slizovskiy, A. P. Rooney, T. Taniguchi, K. Watanabe, S. J. Haigh, V. Fal'ko, I. V. Grigorieva, and I. J. Vera-Marun, Magnetoresistance in co-hbn-nife tunnel junctions enhanced by resonant tunneling through single defects in ultrathin hbn barriers, *Nano Letters* **18**, 6954 (2018).
- [34] E. C. Ahn, 2d materials for spintronic devices, *npj 2D Materials and Applications* **4**, 17 (2020).
- [35] H. Yu, Z. Shao, Y. Tao, X. Jiang, Y. Dong, J. Zhang, Y. Liu, X. Yang, and D. Chen, Tunable tunneling magnetoresistance in in-plane double barrier magnetic tunnel junctions based on b vacancy h-nb nanoribbons, *Physical Chemistry Chemical Physics* **24**, 3451 (2022).
- [36] B. Taudul, M. Bowen, and M. Alouani, Impact of single and double oxygen vacancies on electronic transport in Fe/MgO/Fe magnetic tunnel junctions, *Journal of Applied Physics* **128**, 143902 (2020), https://pubs.aip.org/aip/jap/article-pdf/doi/10.1063/5.0019718/14754077/143902_1_online.pdf.
- [37] A. Kokalj, Xcrysden—a new program for displaying crystalline structures and electron densities, *Journal of Molecular Graphics and Modelling* **17**, 176 (1999).
- [38] D. Sánchez-Portal, P. Ordejón, E. Artacho, and J. M. Soler, Density-functional method for very large systems with lcao basis sets, *International Journal of Quantum Chemistry*, *International Journal of Quantum Chemistry* **65**, 453 (1997).
- [39] J. M. Soler, E. Artacho, J. D. Gale, A. García, J. Junquera, P. Ordejón, and D. Sánchez-Portal, The siesta method for ab initio order-n materials simulation, *Journal of Physics: Condensed Matter* **14**, 2745 (2002).
- [40] N. Troullier and J. Martins, Efficient pseudopotentials for plane-wave calculations, *Physical Review B* **43**, 1993 (1991).
- [41] J. P. Perdew, A. Ruzsinszky, G. I. Csonka, O. A. Vydrov, G. E. Scuseria, L. A. Constantin, X. Zhou, and K. Burke, Restoring the density-gradient expansion for exchange in solids and surfaces, *Phys. Rev. Lett.* **100**, 136406 (2008).
- [42] T. Ozaki and H. Kino, Numerical atomic basis orbitals from h to kr, *Physical Review B* **69**, 195113 (2004).
- [43] T. Ozaki, Variationally optimized atomic orbitals for large-scale electronic structures, *Physical Review B* **67**, 155108 (2003).
- [44] D. Sánchez-Portal, E. Artacho, and J. Soler, Analysis of atomic orbital basis sets from the projection of plane-wave results, *Journal of Physics: Condensed Matter* **8**, 3859 (1996).
- [45] S. Grimme, Semiempirical gga-type density functional constructed with a long-range dispersion correction, *Journal of Computational Chemistry* **27**, 1787 (2006).